HOKKAIDO UNIVERSITY

Title	Zero-field skyrmion, meron, and vortex crystals in centrosymmetric hexagonal magnets
Author(s)	Hayami, Satoru
Citation	Journal of magnetism and magnetic materials, 564(Part 1), 170036 https://doi.org/10.1016/j.jmmm.2022.170036
Issue Date	2022-12-15
Doc URL	https://hdl.handle.net/2115/93772
Rights	© 2022. This manuscript version is made available under the CC-BY-NC-ND 4.0 license https://creativecommons.org/licenses/by-nc-nd/4.0/
Rights(URL)	https://creativecommons.org/licenses/by-nc-nd/4.0/
Type	journal article
File Information	J. Magn. Magn. Mater._564(1)_170036.pdf

Hokkaido University Collection of Scholarly and Academic Papers : HUSCAP

Zero-field skyrmion, meron, and vortex crystals in centrosymmetric hexagonal magnets

Satoru Hayami

Graduate School of Science, Hokkaido University, Sapporo 060-0810, Japan

Abstract

We investigate the interaction conditions to stabilize topological spin textures in centrosymmetric magnets without an external magnetic field. By performing the simulated annealing for an effective spin model with the momentum-resolved interaction on a two-dimensional triangular lattice, we find that the competing interactions between the finite-$\boldsymbol{q}$ channel and the uniform ($\boldsymbol{q} = \boldsymbol{0}$) channel lead to a zero-field skyrmion crystal with the skyrmion number of ± 1. Moreover, we obtain a variety of topological spin textures, such as a meron crystal, vortex crystal, and other multiple-Q states with and without a scalar chirality. We especially show that the bond-dependent anisotropic exchange interaction originating from the relativistic spin-orbit coupling plays an important role in inducing such topological spin textures, while the single-ion anisotropy does not.

Keywords: skyrmion crystal, meron crystal, vortex crystal, multiple-Q magnetic state, triangular lattice, bond-dependent anisotropic interaction

1. Introduction

Spin density waves characterized by a finite-Q ordering vector have long been studied in condensed matter physics, since they give rise to fascinating quantum states of matter and physical phenomena. For example, the spiral ordering with a noncollinear spin texture becomes the origin of intriguing physical phenomena, such as the electric polarization/spin current [1, 2, 3, 4, 5, 6, 7, 8, 9, 10], the antisymmetric spin polarization in the band structure [11, 12, 13], nonreciprocal magnon excitations [14, 15, 16], nonreciprocal transport [17, 18, 19, 20, 21, 22, 23, 24, 25, 26, 27, 28], and emergent inductance [29, 30, 31, 32, 33]. Furthermore, a superposition of spin density waves with a finite-Q ordering vector, which is the so-called multiple-Q state, can induce topological spin textures like the magnetic skyrmion, meron, hedgehog, and vortex crystals, which results in emergent electromagnetic phenomena through the spin Berry phase mechanism [34, 35, 36, 37]. Thus, it is important to clarify the stabilization conditions

Email address: hayami@phys.sci.hokudai.ac.jp (Satoru Hayami)

of the spiral and multiple-Q states based on the theoretical microscopic model, which will be useful in the search for further exotic spin-texture-driven physical phenomena in real materials.

Among them, a magnetic skyrmion crystal (SkX), which is defined as a periodic array of magnetic skyrmion and is characterized as a multiple-Q state, has been extensively studied. Its appearance has been observed in various chemical elements and lattice structures [35]. Accordingly, various mechanisms have been revealed from the theoretical calculations and numerical simulations. The most typical mechanism is the competition between the ferromagnetic exchange interaction and the Dzyaloshinskii-Moriya (DM) interaction in noncentrosymmetric lattice structures [38, 39]. Although the ground-state spin configuration becomes the spiral state, it turns into the SkX when applying an out-of-plane magnetic field [40, 41, 42, 43, 44] as well as an in-plane one [45, 46, 47, 48, 49]. Subsequently, the emergence of such a field-induced SkX has been extended to centrosymmetric lattice structures by focusing on the frustrated short-range exchange interactions [50, 51, 52, 53, 54, 55, 56, 57], frustrated long-range interactions [58, 59, 60, 61], multiple-spin interactions [62, 63, 64, 65, 66, 26, 67, 68], anisotropic exchange interactions [69, 70, 71, 72, 73, 74], dipolar interaction [75, 76], single-ion anisotropy [77, 78, 79], and sublattice-dependent DM interactions [80, 81, 82, 83]. In parallel, the modeling for various skyrmion-hosting materials in both centrosymmetric and noncentrosymmetric lattice structures has been widely developed, which includes the unconventional SkXs with a short magnetic modulation period, such as Gd_2PdSi_3 [84, 85, 86, 87, 88, 89], $Gd_3Ru_4Al_{12}$ [90, 91, 92, 93], $GdRu_2Si_2$ [94, 95, 96], $EuAl_4$ [97, 98, 99, 100], EuPtSi [101, 102, 103, 104], and $MnSc_2S_4$ [105, 106, 107, 108].

In the above mechanisms, the SkX has been often stabilized in the presence of an external magnetic field. This is qualitatively understood from the fact that the magnetic field induces the uniform magnetization proportional to $\boldsymbol{S}_{\boldsymbol{0}}$, which results in an effective coupling in the form of $(\boldsymbol{S}_{\boldsymbol{0}} \cdot \boldsymbol{S}_{\boldsymbol{Q}_1})(\boldsymbol{S}_{\boldsymbol{Q}_2} \cdot \boldsymbol{S}_{\boldsymbol{Q}_3})$ to favor the formation of the triple-Q SkX, where $\boldsymbol{S}_{\boldsymbol{Q}_\eta}$ for η = 1-3 represent the spin with the ordering vectors $\boldsymbol{Q}_\eta$ and $\boldsymbol{Q}_1 + \boldsymbol{Q}_2 + \boldsymbol{Q}_3 = \boldsymbol{0}$ [109]. Indeed, the zero-field SkX is rare compared to the field-induced SkX [110, 111, 112, 113, 114, 115, 116]. In addition, it was shown that the SkX with the skyrmion number of two rather than one tends to be favored in the absence of the magnetic field in centrosymmetric lattice structures [62, 69, 63, 73, 70, 117].

In the present study, we investigate a minimal model to host the SkX with the skyrmion number of one even without the external magnetic field in centrosymmetric magnets. We focus on the competition of the momentum-resolved interactions between the $\boldsymbol{q} = \boldsymbol{0}$ and finite-$\boldsymbol{q}$ channels: The former tends to favor the ferromagnetic state, while the latter tends to favor the spiral state. By performing the simulated annealing for an effective spin model, we show that the SkX can be stabilized at zero field when the interaction in the $\boldsymbol{q} = \boldsymbol{0}$ channel is comparable to that in the finite-$\boldsymbol{q}$ channel, which is in contrast to the previous studies where the SkX appears only under an external magnetic field [72, 93]. We elucidate that the bond-dependent anisotropic exchange interaction also plays an important role in stabilizing the SkX; we could not obtain

the instability toward the SkX under the single-ion anisotropy instead of the bond-dependent anisotropic exchange interaction. Furthermore, we find a variety of other topological spin crystals at zero field; meron crystal, chiral crystal, and vortex crystal, which are described by different multiple-Q superpositions. Our results provide a way of designing zero-field topological spin textures by using the competing interactions at $\boldsymbol{q} = \boldsymbol{0}$ and $\boldsymbol{q} \neq \boldsymbol{0}$.

The remainder of this article is organized as follows. In Sec. 2, we introduce the spin model consisting of the competing interactions in momentum space. We also outline the numerical method based on the simulated annealing. Then, we discuss the magnetic phase diagram of the model in Sec. 3. We show the details of the spin and scalar chirality configurations in various topological spin textures. Section 4 provides a summary. In Appendix A, we present the results in the presence of the easy-axis single-ion anisotropy.

2. Model and method

We consider the following effective spin model on a two-dimensional triangular lattice with the spatial inversion symmetry, whose Hamiltonian is given by

$$\mathcal{H} = -2\sum_{\nu}\sum_{\alpha,\beta} J_{\boldsymbol{Q}_\nu} I^{\alpha\beta}_{\boldsymbol{Q}_\nu} S^{\alpha}_{\boldsymbol{Q}_\nu} S^{\beta}_{-\boldsymbol{Q}_\nu} - J_0 |\boldsymbol{S}_{\boldsymbol{0}}|^2, \tag{1}$$

where $\boldsymbol{S}_i = (S^x_i, S^y_i, S^z_i)$ and $\boldsymbol{S}_{\boldsymbol{Q}_\nu} = (S^x_{\boldsymbol{Q}_\nu}, S^y_{\boldsymbol{Q}_\nu}, S^z_{\boldsymbol{Q}_\nu})$ are the classical localized spin at site i and that with the wave vector $\boldsymbol{q} = \boldsymbol{Q}_\nu$ (ν is the index for the wave vector), respectively, which are related by the Fourier transformation [118]. The magnitude of the localized spin is set to be unity as $|\boldsymbol{S}_i| = 1$. Both the first and second terms stand for the momentum-resolved exchange interaction. The first term corresponds to the finite-$\boldsymbol{q}$ interaction channel ($\boldsymbol{Q}_\nu \neq \boldsymbol{0}$) with the coupling constant $J_{\boldsymbol{Q}_\nu}$; $I^{\alpha\beta}_{\boldsymbol{Q}_\nu}$ describes the anisotropic form factor of the interactions, which depends on the wave vector $\boldsymbol{Q}_\nu$ and spin component $\alpha, \beta = x, y, z$. The anisotropic form factor includes three independent components that are allowed by the symmetry of the triangular lattice under the point group $D_{6\mathrm{h}}$. Among them, we focus on two components: One is an isotropic Heisenberg-type exchange interaction $\delta^{\alpha\beta}$ ($\delta^{\alpha\beta}$ is the Kronecker delta) and the other is a bond-dependent anisotropic exchange interaction $\tilde{I}^{\alpha\beta}_{\boldsymbol{Q}_\nu}$, i.e., $I^{\alpha\beta}_{\boldsymbol{Q}_\nu} = \delta^{\alpha\beta} + \tilde{I}^{\alpha\beta}_{\boldsymbol{Q}_\nu}$. The presence of the latter interaction is due to relativistic spin-orbit coupling and discrete lattice symmetry, which becomes the origin of various topological spin textures in the hexagonal [119, 53, 120, 69, 116], tetragonal [121, 122, 123, 71, 75, 73, 124, 125], and orthorhombic systems [126]. In the main text, we ignore the effect of the single-ion anisotropy, which is also allowed by the symmetry; we discuss such an effect in Appendix A.

The magnitude and sign of $J_{\boldsymbol{Q}_\nu}$ are determined by multiple factors depending on the system. For example, $J_{\boldsymbol{Q}_\nu}$ is related to the short-range exchange interactions in real space between the ith and jth spins J_{ij} in the localized spin model; $J_{\boldsymbol{Q}_\nu} = \sum_{ij} J_{ij} e^{-i\boldsymbol{Q}_\nu\cdot(\boldsymbol{r}_i - \boldsymbol{r}_j)}$ where $\boldsymbol{r}_i$ is the position vector. For another

example, $J_{\boldsymbol{Q}_\nu}$ is related to the long-range exchange interactions in the itinerant electron model. In this case, a complicated wave number dependence of $J_{\boldsymbol{Q}_\nu}$ is obtained according to the electronic band structure like the Ruderman-Kittel-Kasuya-Yosida interaction [127, 128, 129]. In general, the ground-state spin configurations in both cases are not so simple when magnetic frustration including the sign change of the interactions is present.

Meanwhile, the model in Eq. (1) is simplified by focusing on the fact that only a few interaction channels contribute to the energy in the ground-state spin configuration, since the resultant spin configurations are characterized by the single-Q channel or multiple-Q channels to exhibit a few peaks in the spin structure factor in many cases. In other words, it is enough to take into account specific wave vectors $\boldsymbol{Q}_\nu$ that lead to the most dominant components in $J_{\boldsymbol{Q}_\nu}$ in such a situation irrespective of short-range and long-range exchange interactions. Based on this, we consider the interactions only at threefold-symmetric wave vectors owing to the triangular-lattice geometry, i.e., $\boldsymbol{Q}_1 = (Q, 0)$, $\boldsymbol{Q}_2 = (-Q/2, \sqrt{3}Q/2)$, and $\boldsymbol{Q}_3 = (-Q/2, -\sqrt{3}Q/2)$ with $Q = \pi/3$, where the different magnitude of Q also gives a qualitative similar result. Then, $J_{\boldsymbol{Q}_1} = J_{\boldsymbol{Q}_2} = J_{\boldsymbol{Q}_3} \equiv J$, where J is set to be the energy unit of the spin model. Such an approximation by extracting the dominant momentum-resolved interactions enables us to efficiently search for the multiple-Q instability in the model, as clarified in both localized spin model [51, 130, 82, 117, 131, 79] and itinerant electron model [63, 132, 59, 133, 134, 135]. For each $\boldsymbol{Q}_\nu$, the anisotropic form factor $\tilde{I}^{\alpha\beta}_{\boldsymbol{Q}_\nu}$ is given in the form of the symmetric tensor as $-\tilde{I}^{xx}_{\boldsymbol{Q}_1} = \tilde{I}^{yy}_{\boldsymbol{Q}_1} = 2\tilde{I}^{xx}_{\boldsymbol{Q}_2} = -2\tilde{I}^{yy}_{\boldsymbol{Q}_2} = 2\tilde{I}^{xy}_{\boldsymbol{Q}_2}/\sqrt{3} = 2\tilde{I}^{yx}_{\boldsymbol{Q}_2}/\sqrt{3} = 2\tilde{I}^{xx}_{\boldsymbol{Q}_3} = -2\tilde{I}^{yy}_{\boldsymbol{Q}_3} = -2\tilde{I}^{xy}_{\boldsymbol{Q}_3}/\sqrt{3} = -2\tilde{I}^{yx}_{\boldsymbol{Q}_3}/\sqrt{3} \equiv I^{\mathrm{A}}$ [72, 93]. In addition, in contrast to previous studies [72, 93], we here introduce the contribution of the interactions from the $\boldsymbol{q} = \boldsymbol{0}$ component, as represented in the second term in Eq. (1), instead of an out-of-plane external magnetic field. The interaction J_0 plays a similar role to the magnetic field, since they tend to favor the ferromagnetic state. On the other hand, the symmetry of the interaction is different from each other; the interaction J_0 preserves the SU(2) symmetry in spin space, while the magnetic field only preserves the U(1) symmetry. Although the ratio of J_0/J is determined by the real-space exchange interactions and the electronic structures, we take it as the phenomenological parameter in order to investigate the instability toward the topological spin textures in the wide range of the parameter. As detailed in Sec. 3, the competition of the interactions between $\boldsymbol{q} = \boldsymbol{0}$ and $\boldsymbol{q} = \boldsymbol{Q}_\nu$ is essential to induce the topological spin textures at zero field.

The low-temperature optimal spin configurations of the model in Eq. (1) under these considerations are calculated by performing the simulated annealing with the Metropolis local updates for localized spins in real space [136]. Starting from a random spin configuration at high temperatures T_0 = 1-10, we gradually reduce the temperature to the target low temperature $T_f = 0.001$, where we set the annealing rate as $\alpha = 0.99999$-0.999999 and $T_{n+1} = \alpha T_n$ in each Monte Carlo step. At T_f, we perform 10^5-10^6 Monte Carlo sweeps for measurements after equilibration. We independently perform the simulations in each set of

model parameters. In the parameter region close to the phase boundaries, we also perform the simulations by starting the spin configurations obtained at low temperatures. The system size is taken as $N = 24^2$ in the following calculations.

The magnetic phases are distinguished from the spin and scalar chirality configurations. The spin structure factor is defined as

$$S_s(\boldsymbol{q}) = \sum_{\alpha} S_s^{\alpha\alpha}(\boldsymbol{q}), \tag{2}$$

$$S_s^{\alpha\alpha}(\boldsymbol{q}) = \frac{1}{N}\sum_{i,j}\langle S_i^{\alpha} S_j^{\alpha}\rangle e^{i\boldsymbol{q}\cdot(\boldsymbol{r}_i-\boldsymbol{r}_j)}, \tag{3}$$

where $\alpha = x, y, z$ and $\langle\cdots\rangle$ corresponds to the average over the Monte Carlo samplings. The net magnetization is given by $M = \sqrt{(M^x)^2 + (M^y)^2 + (M^z)^2}$ with $M^{\alpha} = (1/N)\sum_i S_i^{\alpha}$. We also calculate the spin scalar chirality, which is defined by

$$S_{\chi}(\boldsymbol{q}) = \frac{1}{N}\sum_{\mu}\sum_{\boldsymbol{R},\boldsymbol{R}'\in\mu}\chi_{\boldsymbol{R}}\chi_{\boldsymbol{R}'}e^{i\boldsymbol{q}\cdot(\boldsymbol{R}-\boldsymbol{R}')}, \tag{4}$$

$$\chi_{\boldsymbol{R}} = \boldsymbol{S}_i\cdot(\boldsymbol{S}_j\times\boldsymbol{S}_k), \tag{5}$$

where $\mu = (u, d)$ denotes upward and downward triangles, respectively, and $\chi_{\boldsymbol{R}}$ represents the local spin scalar chirality at the triangle center $\boldsymbol{R}$ consisting of spins at i, j, and k in the counterclockwise order. We show the uniform component of $S_{\chi}(\boldsymbol{q})$, i.e., $S_{\chi}(\boldsymbol{0})/N \equiv \chi$. The nonzero scalar chirality leads to the emergence of the Hall effect even neither a net magnetization nor the spin-orbit coupling.

3. Results

Figure 1 shows the magnetic phase diagram obtained by the simulated annealing while changing the ferromagnetic interaction J_0 and bond-dependent anisotropic form factor I^{A}. The phase boundaries are drawn from the data obtained at $\Delta J_0 = 0.01$ and $\Delta I^{\mathrm{A}} = 0.02$. There are eight phases in addition to the ferromagnetic phase denoted as FM in the phase diagram; Q' in the phases means the different amplitudes among the constituent waves, as detailed below. In the ferromagnetic phase, the moments are fully-polarized but their direction is arbitrary owing to the isotropic interaction at $\boldsymbol{q} = \boldsymbol{0}$. It is noted that the phase boundaries between double-Q' chiral stripe (CS) and double-Q vertical spiral (VS) and between double-Q vertical spiral and double-Q' coplanar state are unchanged for $J_0 < 1$, which connects the result obtained for $J_0 = 0$ [72].

In the following, we describe the details of the spin and scalar chirality quantities in each phase one by one; the real-space spin and scalar chirality configurations are shown in Fig. 2 and the spin structure factors are shown in Fig. 3. We also present the I^{A} dependence of the magnetization M and scalar chirality χ for several J_0 in Fig. 4.

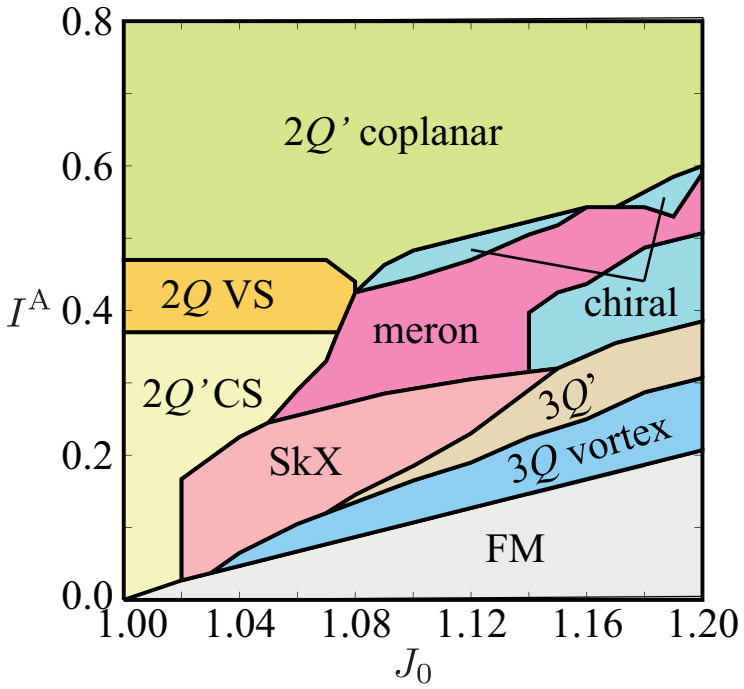


Figure 1: Phase diagram in the plane of the uniform component of the interaction J_0 and the bond-dependent anisotropic form factor I^{A} obtained by the simulated annealing. SkX, CS, VS, and FM represent the skyrmion crystal, chiral stripe, vertical spiral, and ferromagnetic states, respectively. $2Q$ and $3Q$ represent the double-Q and triple-Q states, respectively, where Q' means the different amplitudes of the constituent waves.

2Q′ chiral stripe (2Q′ CS). This state appears in the small I^{A} region for $J_0 \lesssim 1.08$. The spin configuration is characterized by a double-Q noncoplanar superposition with different intensities: the spiral state along the $\boldsymbol{Q}_3$ direction and the sinusoidal modulation along the $\boldsymbol{Q}_1$ direction, as shown in the left panel of Fig. 2(a). It is noted that the choice of $\boldsymbol{Q}_1$, $\boldsymbol{Q}_2$, $\boldsymbol{Q}_3$ is arbitrary owing to the threefold rotational symmetry. The dominant intensity arises from the spiral modulation at $\boldsymbol{Q}_3$, as shown by the spin structure factor in Fig. 3(a). Due to the noncoplanar spin structure, this state accompanies the density wave in terms of the scalar chirality along the $\boldsymbol{Q}_1$ direction, as shown in the right panel of Fig. 2(a). Meanwhile, this state does not have a net component of scalar chirality, i.e., $\chi = 0$. Similar states have been found in the Kondo lattice model [137, 138, 139] and d-p model [140] even without the anisotropic exchange interaction.

2Q vertical spiral (2Q VS). This state is stabilized next to the double-Q' chiral stripe state by increasing I^{A} in Fig. 1. In contrast to the double-Q' chiral stripe state, this state shows the double-Q peak structures with equal intensity. For example, in the case of $J_0 = 1.02$ and $I^{\mathrm{A}} = 0.4$, the double-Q peaks are

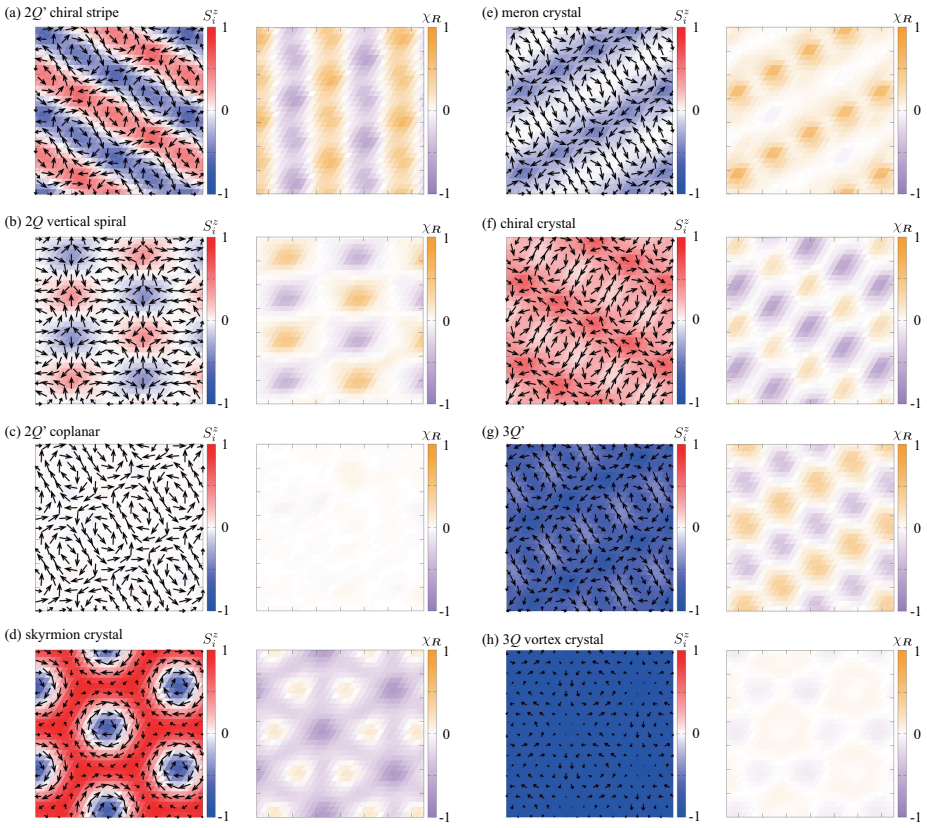


Figure 2: The real-space spin (left panel) and scalar chirality (right panel) configurations in (a) the double-Q' ($2Q'$) chiral stripe state at $J_0 = 1.02$ and $I^{\rm A} = 0.3$, (b) the $2Q$ vertical spiral state at $J_0 = 1.02$ and $I^{\rm A} = 0.4$, (c) the $2Q'$ coplanar state at $J_0 = 1.1$ and $I^{\rm A} = 0.6$, (d) the skyrmion crystal at $J_0 = 1.06$ and $I^{\rm A} = 0.2$, (e) the meron crystal at $J_0 = 1.1$ and $I^{\rm A} = 0.4$, (f) the chiral crystal at $J_0 = 1.16$ and $I^{\rm A} = 0.4$, (g) the triple-Q' ($3Q'$) state at $J_0 = 1.16$ and $I^{\rm A} = 0.3$, and (h) the $3Q$ vortex crystal at $J_0 = 1.08$ and $I^{\rm A} = 0.1$. In the left panel, the arrows and the color show the xy and z components of spins, respectively.

located at $\boldsymbol{Q}_2$ and $\boldsymbol{Q}_3$, as shown in Fig. 3(b). From the real-space picture in the left panel of Fig. 2(b), one finds the spiral spin modulation at $\boldsymbol{Q}_2$ and $\boldsymbol{Q}_3$, which leads to the periodic alignment of the vortices with $S_i^z = 1$ and $S_i^z = -1$ like the meron-antimeron crystal. Here, the meron and antimeron represent the topological objects with an opposite sign of a half skyrmion number, where spins around the vortices wrap only half of the sphere in spin space [141, 142, 143, 144, 145]. Such a meron-like feature is also found in the scalar chirality in the right panel of Fig. 2(b); there is a negative (positive) chirality around the meron (antimeron), and the total chirality becomes zero.

2Q′ coplanar. The double-Q' coplanar state appears in the region for large $I^{\rm A}$ irrespective of J_0 in Fig. 1. The spin configuration in this state is charac-

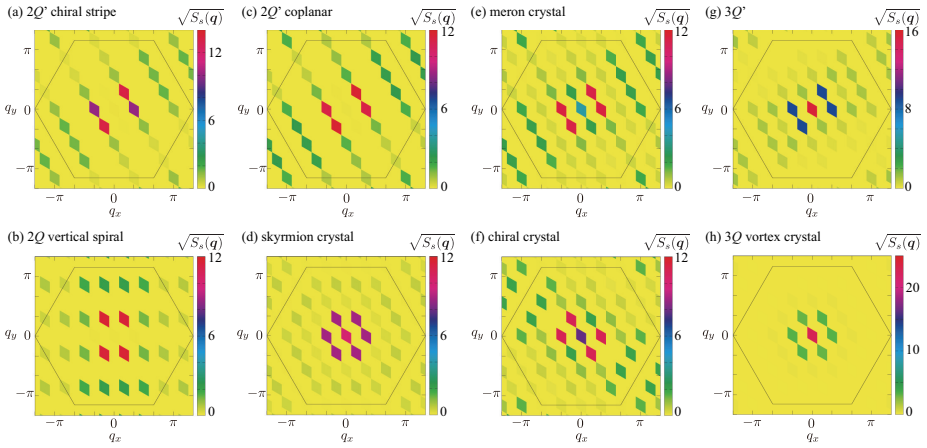


Figure 3: The square root of the the spin structure factor in (a) the $2Q'$ chiral stripe state at $J_0 = 1.02$ and $I^{\rm A} = 0.3$, (b) the $2Q$ vertical spiral state at $J_0 = 1.02$ and $I^{\rm A} = 0.4$, (c) the $2Q'$ coplanar state at $J_0 = 1.1$ and $I^{\rm A} = 0.6$, (d) the skyrmion crystal at $J_0 = 1.06$ and $I^{\rm A} = 0.2$, (e) the meron crystal at $J_0 = 1.1$ and $I^{\rm A} = 0.4$, (f) the chiral crystal at $J_0 = 1.16$ and $I^{\rm A} = 0.4$, (g) the $3Q'$ state at $J_0 = 1.16$ and $I^{\rm A} = 0.3$, and (h) the $3Q$ vortex crystal at $J_0 = 1.08$ and $I^{\rm A} = 0.1$. Black hexagons represent the first Brillouin zone.

terized by a double-Q superposition of the sinusoidal waves with the different spin components in the xy plane. The intensities of the spin structure factor at the double-Q peak are almost the same in the small $I^{\rm A}$ region, but they are slightly different while increasing $I^{\rm A}$ [72]; we do not distinguish such a subtle difference for simplicity. The spin structure factor at $J_0 = 1.1$ and $I^{\rm A} = 0.6$ with almost the same intensities at $\boldsymbol{Q}_1$ and $\boldsymbol{Q}_3$ is shown in Fig. 3(c). We present the real-space spin configuration in the left panel of Fig. 2(c), where a periodic alignment of the vortex and antivortex is found. Thus, one finds that the in-plane spin modulation in the double-Q' coplanar state is similar to that in the double-Q' chiral stripe state, while the z-spin modulation is different from each other. Accordingly, there is no chirality density wave in this state, as shown in the right panel of Fig. 2(c).

Skyrmion crystal (SkX). While increasing J_0 in the $2Q'$ chiral stripe state, the SkX is stabilized for small $I^{\rm A}$ in Fig. 1. The spin configuration in the left panel of Fig. 2(d) is similar to that under an external magnetic field [72]; the skyrmion cores with $S_i^z = -1$, which are located at the center of the triangle owing to the discrete-lattice structure [146], form the triangular lattice. However, it is noted that the SkX with the skyrmion core at $S_i^z = +1$ is degenerate due to the absence of the magnetic field; in numerical simulations, both states are obtained depending on the initial spin configuration. In other words, there are two types of the SkXs at zero field, either of which is selected through a spontaneous phase transition. Meanwhile, the helicity of each skyrmion core is determined by the sign of the anisotropic exchange interaction $I^{\rm A}$; $I^{\rm A} > 0$ leads to the Bloch-type SkX and $I^{\rm A} < 0$ leads to the Néel-type SkX. In momen-

tum space, the spin configuration is characterized by a triple-Q superposition of proper-screw spiral waves at $\boldsymbol{Q}_1$, $\boldsymbol{Q}_2$, and $\boldsymbol{Q}_3$ with equal intensity, as shown in Fig. 3(d). The linear combination of the triple-Q spiral waves leads to the uniform magnetization at $\boldsymbol{q} = \boldsymbol{0}$ in the spin structure factor. The polarized direction depends on the z-spin direction at the skyrmion core; $M > 0$ ($M < 0$) for the negative (positive) z-spin polarization at the core. In the scalar chirality, the SkX exhibits a quantized skyrmion number of ± 1 in the magnetic unit cell, where its sign also depends on the z-spin direction at the skyrmion core. We here denote the SkX with -1 ($+1$) as the SkX (anti-SkX) to distinguish them. In the case of Fig. 2(d), the SkX is realized, where the skyrmion number is quantized as -1. The degeneracy between the SkXs with ± 1 might imply a possibility of the coexistence of the SkX and anti-SkX, as found in the spin model at finite temperatures [50, 60, 61].

The realization of the zero-field SkX is due to the interplay between the bond-dependent anisotropic exchange interaction I^{A} and the ferromagnetic exchange interaction J_0. Specifically, there are mainly two important conditions: One is the presence of the bond-dependent anisotropic exchange interaction that arises from the relativistic spin-orbit coupling in the discrete lattice structure. Indeed, when introducing the other type of magnetic anisotropy, such as single-ion anisotropy, there is no longer the SkX phase, as discussed in Appendix A. The other is that the interaction at $\boldsymbol{q} = \boldsymbol{0}$ is slightly larger than that at $\boldsymbol{q} = \boldsymbol{Q}_\nu$, which means that the ground-state spin configuration is the ferromagnetic state for $I^{\mathrm{A}} = 0$. Intriguingly, these two conditions also give rise to other multiple-Q states, the meron crystal, chiral crystal, and triple-Q vortex crystal, as will be discussed below.

Meron crystal. The meron crystal is stabilized in the region next to the SkX while increasing I^{A} in Fig. 1. As shown in the spin configuration in the left panel of Fig. 2(e), the modulation of the in-plane spin component is similar to that in the double-Q' chiral stripe [Fig. 2(a)] and double-Q' coplanar state [Fig. 2(c)]; there are dominant double-Q modulations with $\boldsymbol{Q}_1$ and $\boldsymbol{Q}_3$. Meanwhile, this state shows the subdominant z-spin modulation along the $\boldsymbol{Q}_2$ direction, as shown in Fig. 3(e). As a result, there is a local z-spin polarization around the antivortex while keeping almost no z-spin polarization around the vortex, which leads to an imbalance between them in terms of the scalar chirality: The former antivortex accompanies the positive scalar chirality, while the latter vortex does not show the scalar chirality, as shown in the right panel of Fig. 2(e). Indeed, when we calculate the skyrmion number, this state exhibits the skyrmion number of 1, since there are two antivortices with a half skyrmion number in the magnetic unit cell. Thus, this state is regarded as a meron crystal consisting of a periodic alignment of two types of meron with a half skyrmion number. Although a similar meron crystal is also realized in an external magnetic field [72], our result indicates that the competition between the bond-dependent anisotropic exchange interaction and the ferromagnetic uniform interaction also stabilizes such states even without the magnetic field.

Chiral crystal. The chiral crystal appears in the vicinity of the meron crystal in the phase diagram in Fig. 1. The overall spin configuration in this state is

similar to that in the meron crystal as compared to the left panel of Figs. 2(e) and 2(f). On the other hand, one finds that the vortex core also exhibits the z-spin polarization in the chiral crystal. Accordingly, the opposite sign of the scalar chirality is induced, as shown in the right panel of Fig. 2(f). Then, the total scalar chirality tends to be smaller owing to the cancellation; the skyrmion number becomes zero or a non-quantized number less than one, the latter of which might be attributed to the short-period magnetic modulations on a discrete lattice structure. Reflecting the similarity of the real-space spin textures between the chiral crystal and meron crystal, the spin structure factor also resembles each other, as shown in Figs. 3(e) and 3(f).

3Q' state. The triple-Q' state appears while decreasing $I^{\rm A}$ in the chiral crystal, as shown in Fig. 1. This state also shows a similar spin texture to the meron and chiral crystals. According to the decrease of $I^{\rm A}$, the spins have a more z-spin polarization in the vortex core, which leads to almost no z-spin modulation in this state shown in the left panel of Fig. 2(g). This results in the same magnitude of the positive and negative scalar chirality, as shown in the right panel of Fig. 2(g). We identify the $3Q'$ state when $(\sum_{\boldsymbol{R}} \chi_{\boldsymbol{R}}/N)^2$ is less than 0.005 quantitatively. The spin structure factor in Fig. 3(g) is similar to that in the meron crystal in Fig. 3(e) and the chiral crystal in Fig. 3(f).

3Q vortex crystal. The $3Q$ vortex crystal is stabilized in the region for large J_0 and small $I^{\rm A}$ in Fig. 1. The spin configuration in this state is mainly characterized by the in-plane triple-Q superposition in addition to the uniform magnetization along the z direction, as shown in the left panel of Fig. 2(h). The amplitudes of the triple-Q spin density waves are the same as found in the spin structure factor in Fig. 3(h). Meanwhile, there is no uniform scalar chirality shown in the right panel of Fig. 2(h). A similar state has been stabilized in the spin model by taking into account quantum fluctuations [147] and nonmagnetic impurities [55], where its instability appears in the vicinity of the fully-polarized state under the magnetic field.

Finally, let us discuss the $I^{\rm A}$ dependence of the magnetization M and the scalar chirality χ for different values of J_0 in Fig. 4. For $I^{\rm A} = 1.03$ in Fig. 4(a), the ferromagnetic state with the full magnetization ($M = 1$) is stabilized at $I^{\rm A} \lesssim 0.03$. While increasing $I^{\rm A}$, the magnetization deviates from $M = 1$, which indicates the transition from the ferromagnetic state to the triple-Q vortex crystal. Then, the SkX with both nonzero M and χ at $I^{\rm A} = 0.06$ is stabilized while showing their jumps. While further increasing $I^{\rm A}$, the ground state changes from the SkX to the double-Q' chiral stripe, double-Q vertical spiral, and double-Q' coplanar state neither M nor χ; they are distinguished by the nonuniform spin and chirality configurations as discussed above.

For larger J_0 in Figs. 4(b) and 4(c), the magnetic phases with large M tend to extend in order to gain the energy by J_0. One finds that there are jumps of M and χ between the SkX and the meron crystal. Meanwhile, they continuously change from the meron crystal to the chiral crystal in spite of the different skyrmion numbers, which might be owing to their similarity in terms of the spin and chirality textures, as discussed above. This result implies that the topological feature of the SkX is more robust compared to that of the meron

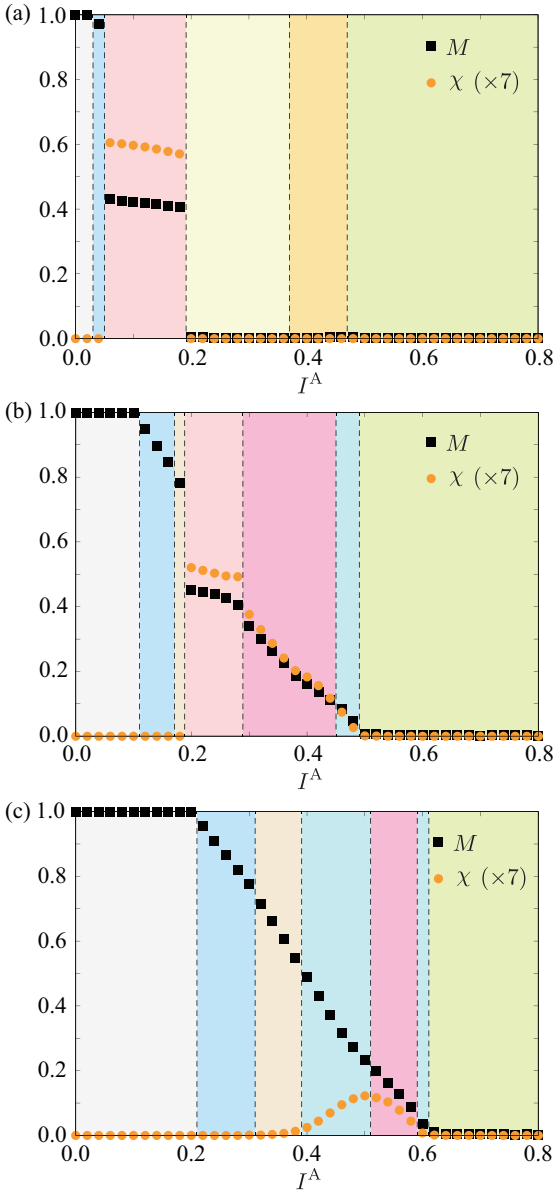


Figure 4: I^{A} dependence of the magnetization M and the scalar chirality χ for (a) $J_0 = 1.03$, (b) $J_0 = 1.1$, and (c) $J_0 = 1.2$. The colors in the background correspond to those in Fig. 1.

crystal.

4. Summary

To summarize, we have investigated the stabilization of the zero-field topological spin textures with an emphasis on the competition of the interactions between finite-$\boldsymbol{q}$ and $\boldsymbol{q} = \boldsymbol{0}$ components. By carrying out the simulated annealing for the effective spin model with the momentum-resolved interaction on a centrosymmetric triangular lattice, we find that the interplay between the bond-dependent anisotropic exchange interaction and the ferromagnetic interaction gives rise to rich multiple-Q states, such as the SkX, meron crystal, chiral crystal, and vortex crystal, even at zero field. As the bond-dependent anisotropic exchange interaction originates from the relativistic spin-orbit coupling, our results indicate that magnetic materials with strong spin-orbit coupling are candidates to exhibit zero-field topological spin textures.

One of the candidate systems is the heterostructure consisting of two magnetic layers: One is the magnetic layer (layer A) with the frustrated exchange interaction so that the ground state becomes the spiral ordering. The other is the ferromagnetic layer (layer B). When the proximity effect between them is taken into account, the spins on layer A feel the ferromagnetic exchange interaction through the coupling to those on layer B, which corresponds to a similar situation in the model in Eq. (1).

This research was supported by JSPS KAKENHI Grants Numbers JP21H01037, JP22H04468, JP22H00101, JP22H01183, and by JST PRESTO (JPMJPR20L8). Parts of the numerical calculations were performed in the supercomputing systems in ISSP, the University of Tokyo.

Appendix A. Results of easy-axis single-ion anisotropy

In this Appendix, we show that the single-ion anisotropy does not lead to the instability toward the zero-field multiple-Q states in contrast to the bond-dependent anisotropic exchange interaction. For the model in Eq. (1), we additionally consider the effect of the single-ion anisotropy, which is given by

$$\mathcal{H}^{\mathrm{SIA}} = -A\sum_i (S_i^z)^2, \tag{A.1}$$

where we take $A > 0$. We also take $I^{\mathrm{A}} = 0$ to focus on the role of A.

Figure A.5 shows the magnetic phase diagram in the plane of J_0 and A obtained by the simulated annealing. As shown in the phase diagram, only the single-Q states appear in addition to the ferromagnetic state. For small A, the single-Q vertical spiral state is realized, and it is replaced by the single-Q collinear state while increasing A. This result shows that the bond-dependent anisotropic exchange interaction I^{A} introduced in the main text plays an essential role in inducing the zero-field SkX and other topological spin textures.

In addition, these results clearly indicate the difference between the ferromagnetic interaction J_0 and the external magnetic field on the stabilization of the SkX. This is because the SkX is stabilized in the system with the easy-axis

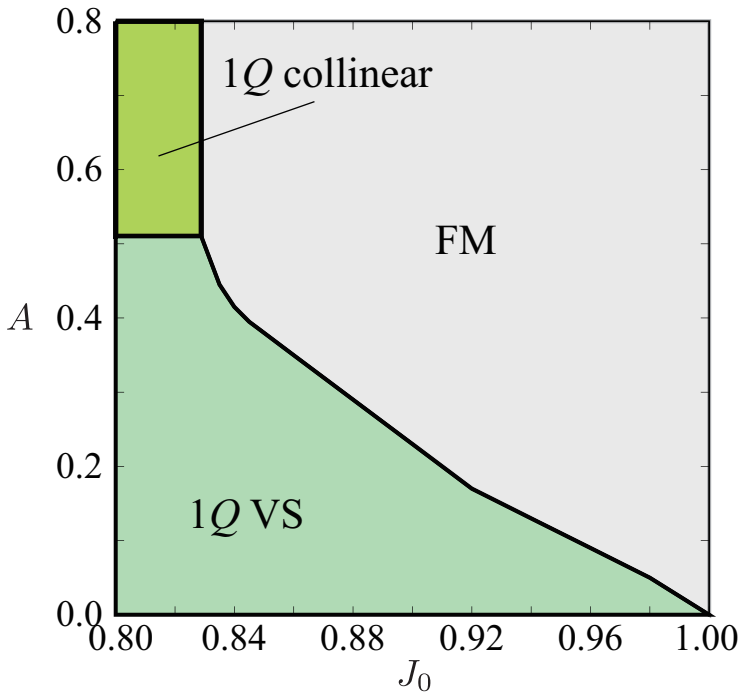


Figure A.5: Magnetic phase diagram in the presence of the single-ion anisotropy (A) instead of the bond-dependent anisotropy I^{A}. VS and FM represent the vertical spiral and ferromagnetic states, respectively.

single-ion anisotropy only when considering the effect of the external magnetic field [51, 52, 77].

References

[1] H. Katsura, N. Nagaosa, A. V. Balatsky, Spin current and magnetoelectric effect in noncollinear magnets, Phys. Rev. Lett. 95 (2005) 057205. doi:10.1103/PhysRevLett.95.057205.

[2] M. Mostovoy, Ferroelectricity in spiral magnets, Phys. Rev. Lett. 96 (2006) 067601. doi:10.1103/PhysRevLett.96.067601.

[3] S.-W. Cheong, M. Mostovoy, Multiferroics: a magnetic twist for ferroelectricity, Nat. Mater. 6 (1) (2007) 13–20. doi:10.1038/nmat1804.

[4] L. N. Bulaevskii, C. D. Batista, M. V. Mostovoy, D. I. Khomskii, Electronic orbital currents and polarization in mott insulators, Phys. Rev. B 78 (2008) 024402. doi:10.1103/PhysRevB.78.024402.

[5] S. Seki, X. Z. Yu, S. Ishiwata, Y. Tokura, Observation of skyrmions in a multiferroic material, Science 336 (6078) (2012) 198–201. doi:10.1126/science.1214143.

[6] J. S. White, I. Levatić, A. Omrani, N. Egetenmeyer, K. Prša, I. Živković, J. L. Gavilano, J. Kohlbrecher, M. Bartkowiak, H. Berger, et al., Electric field control of the skyrmion lattice in cu2oseo3, J. Phys.: Condens. Matter 24 (43) (2012) 432201. doi:10.1088/0953-8984/24/43/432201.

[7] Y. Tokura, S. Seki, N. Nagaosa, Multiferroics of spin origin, Rep. Prog. Phys. 77 (7) (2014) 076501. doi:10.1088/0034-4885/77/7/076501.

[8] M. Mochizuki, S. Seki, Dynamical magnetoelectric phenomena of multiferroic skyrmions, J. Phys.: Condens. Matter 27 (50) (2015) 503001. doi:10.1088/0953-8984/27/50/503001.

[9] B. Göbel, A. Mook, J. Henk, I. Mertig, Magnetoelectric effect and orbital magnetization in skyrmion crystals: Detection and characterization of skyrmions, Phys. Rev. B 99 (2019) 060406. doi:10.1103/PhysRevB.99.060406.

[10] T. Kurumaji, Spiral spin structures and skyrmionsin multiferroics, Phys. Sci. Rev. 5 (2020) 20190016. doi:10.1515/psr-2019-0016.

[11] S. Hayami, Y. Yanagi, H. Kusunose, Spontaneous antisymmetric spin splitting in noncollinear antiferromagnets without spin-orbit coupling, Phys. Rev. B 101 (2020) 220403(R). doi:10.1103/PhysRevB.101.220403.

[12] S. Hayami, Y. Yanagi, H. Kusunose, Bottom-up design of spin-split and reshaped electronic band structures in antiferromagnets without spin-orbit coupling: Procedure on the basis of augmented multipoles, Phys. Rev. B 102 (2020) 144441. doi:10.1103/PhysRevB.102.144441.

[13] S. Hayami, Mechanism of antisymmetric spin polarization in centrosymmetric multiple-q magnets based on effective chiral bilinear and biquadratic spin cross products, Phys. Rev. B 105 (2022) 024413. doi:10.1103/PhysRevB.105.024413.

[14] S. Miyahara, N. Furukawa, Nonreciprocal directional dichroism and toroidalmagnons in helical magnets, J. Phys. Soc. Jpn. 81 (2) (2012) 023712. doi:10.1143/JPSJ.81.023712.

[15] S. Miyahara, N. Furukawa, Theory of magneto-optical effects in helical multiferroic materials via toroidal magnon excitation, Phys. Rev. B 89 (2014) 195145. doi:10.1103/PhysRevB.89.195145.

[16] T. Matsumoto, S. Hayami, Nonreciprocal magnon excitations by the dzyaloshinskii-moriya interaction on the basis of bond magnetic toroidal multipoles, Phys. Rev. B 104 (2021) 134420. doi:10.1103/PhysRevB.104.134420.

[17] S. Seki, Y. Okamura, K. Kondou, K. Shibata, M. Kubota, R. Takagi, F. Kagawa, M. Kawasaki, G. Tatara, Y. Otani, Y. Tokura, Magnetochiral nonreciprocity of volume spin wave propagation in chiral-lattice ferromagnets, Phys. Rev. B 93 (2016) 235131. doi:10.1103/PhysRevB.93.235131.

[18] A. Giordano, R. Verba, R. Zivieri, A. Laudani, V. Puliafito, G. Gubbiotti, R. Tomasello, G. Siracusano, B. Azzerboni, M. Carpentieri, A. Slavin, G. Finocchio, Spin-hall nano-oscillator with oblique magnetization and dzyaloshinskii-moriya interaction as generator of skyrmions and nonreciprocal spin-waves, Sci. Rep. 6 (2016) 36020. doi:10.1038/srep36020.

[19] Y. Tokura, N. Nagaosa, Nonreciprocal responses from non-centrosymmetric quantum materials, Nat. Commun. 9 (1) (2018) 3740. doi:10.1038/s41467-018-05759-4.

[20] T. Yokouchi, S. Hoshino, N. Kanazawa, A. Kikkawa, D. Morikawa, K. Shibata, T.-h. Arima, Y. Taguchi, F. Kagawa, N. Nagaosa, Y. Tokura, Current-induced dynamics of skyrmion strings, Sci. Adv. 4 (8) (2018) eaat1115. doi:10.1126/sciadv.aat1115.

[21] S. Hoshino, N. Nagaosa, Theory of the magnetic skyrmion glass, Phys. Rev. B 97 (2018) 024413. doi:10.1103/PhysRevB.97.024413.

[22] V. G. Bar'yakhtar, A. G. Danilevich, V. N. Krivoruchko, Magnetochiral nonreciprocity of spin wave damping in long-period structures, Phys. Rev. B 99 (2019) 104407. doi:10.1103/PhysRevB.99.104407.

[23] S. Okumura, H. Ishizuka, Y. Kato, J.-i. Ohe, Y. Motome, Spin-current diode with a monoaxial chiral magnet, Appl. Phys. Lett. 115 (1) (2019) 012401. doi:10.1063/1.5097866.

[24] F. J. dos Santos, M. dos Santos Dias, S. Lounis, Nonreciprocity of spin waves in noncollinear magnets due to the dzyaloshinskii-moriya interaction, Phys. Rev. B 102 (2020) 104401. doi:10.1103/PhysRevB.102.104401.

[25] S. Seki, M. Garst, J. Waizner, R. Takagi, N. Khanh, Y. Okamura, K. Kondou, F. Kagawa, Y. Otani, Y. Tokura, Propagation dynamics of spin excitations along skyrmion strings, Nat. Commun. 11 (2020) 256. doi:10.1038/s41467-019-14095-0.

[26] S. Hayami, T. Okubo, Y. Motome, Phase shift in skyrmion crystals, Nat. Commun. 12 (2021) 6927. doi:10.1038/s41467-021-27083-0.

[27] S. Hayami, M. Yatsushiro, Nonlinear nonreciprocal transport in antiferromagnets free from spin-orbit coupling, Phys. Rev. B 106 (2022) 014420. doi:10.1103/PhysRevB.106.014420.

[28] S. Hayami, M. Yatsushiro, Nonreciprocal transport in noncoplanar magnetic systems without spin-orbit coupling, net scalar chirality, or magnetization, J. Phys. Soc. Jpn. 91 (9) (2022) 094704. doi:10.7566/JPSJ.91.094704.

[29] N. Nagaosa, Emergent inductor by spiral magnets, Japan J. Appl. Phys. 58 (12) (2019) 120909. doi:10.7567/1347-4065/ab5294.

[30] T. Yokouchi, F. Kagawa, M. Hirschberger, Y. Otani, N. Nagaosa, Y. Tokura, Emergent electromagnetic induction in a helical-spin magnet, Nature 586 (7828) (2020) 232–236. doi:10.1038/s41586-020-2775-x.

[31] J. Ieda, Y. Yamane, Intrinsic and extrinsic tunability of rashba spin-orbit coupled emergent inductors, Phys. Rev. B 103 (2021) L100402. doi:10.1103/PhysRevB.103.L100402.

[32] D. Kurebayashi, N. Nagaosa, Electromagnetic response in spiral magnets and emergent inductance, Commun. Phys. 4 (2021) 260. doi:10.1038/s42005-021-00765-3.

[33] A. Kitaori, N. Kanazawa, T. Yokouchi, F. Kagawa, N. Nagaosa, Y. Tokura, Emergent electromagnetic induction beyond room temperature, Proc. Natl. Acad. Sci. U.S.A. 118 (33) (2021). doi:10.1073/pnas.2105422118.

[34] N. Nagaosa, Y. Tokura, Topological properties and dynamics of magnetic skyrmions, Nat. Nanotechnol. 8 (12) (2013) 899–911. doi:10.1038/nnano.2013.243.

[35] Y. Tokura, N. Kanazawa, Magnetic skyrmion materials, Chem. Rev. 121 (2021) 2857. doi:10.1021/acs.chemrev.0c00297.

[36] S. Hayami, Y. Motome, Topological spin crystals by itinerant frustration, J. Phys.: Condens. Matter 33 (44) (2021) 443001. doi:10.1088/1361-648x/ac1a30.

[37] B. Göbel, I. Mertig, O. A. Tretiakov, Beyond skyrmions: Review and perspectives of alternative magnetic quasiparticles, Phys. Rep. 895 (2021) 1. doi:10.1016/j.physrep.2020.10.001.

[38] I. Dzyaloshinsky, A thermodynamic theory of "weak" ferromagnetism of antiferromagnetics, J. Phys. Chem. Solids 4 (4) (1958) 241–255.

[39] T. Moriya, Anisotropic superexchange interaction and weak ferromagnetism, Phys. Rev. 120 (1) (1960) 91.

[40] U. K. Rößler, A. N. Bogdanov, C. Pfleiderer, Spontaneous skyrmion ground states in magnetic metals, Nature 442 (7104) (2006) 797–801. doi:10.1038/nature05056.

[41] B. Binz, A. Vishwanath, V. Aji, Theory of the helical spin crystal: A candidate for the partially ordered state of mnsi, Phys. Rev. Lett. 96 (2006) 207202. doi:10.1103/PhysRevLett.96.207202.

[42] B. Binz, A. Vishwanath, Theory of helical spin crystals: Phases, textures, and properties, Phys. Rev. B 74 (2006) 214408. doi:10.1103/PhysRevB.74.214408.

[43] S. D. Yi, S. Onoda, N. Nagaosa, J. H. Han, Skyrmions and anomalous hall effect in a dzyaloshinskii-moriya spiral magnet, Phys. Rev. B 80 (2009) 054416. doi:10.1103/PhysRevB.80.054416.

[44] A. B. Butenko, A. A. Leonov, U. K. Rößler, A. N. Bogdanov, Stabilization of skyrmion textures by uniaxial distortions in noncentrosymmetric cubic helimagnets, Phys. Rev. B 82 (2010) 052403. doi:10.1103/PhysRevB.82.052403.

[45] B. Göbel, A. Mook, J. Henk, I. Mertig, O. A. Tretiakov, Magnetic bimerons as skyrmion analogues in in-plane magnets, Phys. Rev. B 99 (2019) 060407(R). doi:10.1103/PhysRevB.99.060407.

[46] K.-W. Moon, J. Yoon, C. Kim, C. Hwang, Existence of in-plane magnetic skyrmion and its motion under current flow, Phys. Rev. Applied 12 (2019) 064054. doi:10.1103/PhysRevApplied.12.064054.

[47] L. Shen, X. Li, J. Xia, L. Qiu, X. Zhang, O. A. Tretiakov, M. Ezawa, Y. Zhou, Dynamics of ferromagnetic bimerons driven by spin currents and magnetic fields, Phys. Rev. B 102 (2020) 104427. doi:10.1103/PhysRevB.102.104427.

[48] L. Flacke, V. Ahrens, S. Mendisch, L. Körber, T. Böttcher, E. Meidinger, M. Yaqoob, M. Müller, L. Liensberger, A. Kákay, M. Becherer, P. Pirro, M. Althammer, S. Geprägs, H. Huebl, R. Gross, M. Weiler, Robust formation of nanoscale magnetic skyrmions in easy-plane anisotropy thin film multilayers with low damping, Phys. Rev. B 104 (2021) L100417. doi:10.1103/PhysRevB.104.L100417.

[49] S. Hayami, R. Yambe, Skyrmion crystal under D_{3h} point group: Role of out-of-plane dzyaloshinskii-moriya interaction, Phys. Rev. B 105 (2022) 224423. doi:10.1103/PhysRevB.105.224423.

[50] T. Okubo, S. Chung, H. Kawamura, Multiple-q states and the skyrmion lattice of the triangular-lattice heisenberg antiferromagnet under magnetic fields, Phys. Rev. Lett. 108 (2012) 017206. doi:10.1103/PhysRevLett.108.017206.

[51] A. O. Leonov, M. Mostovoy, Multiply periodic states and isolated skyrmions in an anisotropic frustrated magnet, Nat. Commun. 6 (2015) 8275. doi:10.1038/ncomms9275.

[52] S.-Z. Lin, S. Hayami, Ginzburg-landau theory for skyrmions in inversion-symmetric magnets with competing interactions, Phys. Rev. B 93 (2016) 064430. doi:10.1103/PhysRevB.93.064430.

[53] I. Rousochatzakis, U. K. Rössler, J. van den Brink, M. Daghofer, Kitaev anisotropy induces mesoscopic Z_2 vortex crystals in frustrated hexagonal antiferromagnets, Phys. Rev. B 93 (2016) 104417. doi:10.1103/PhysRevB.93.104417.

[54] C. D. Batista, S.-Z. Lin, S. Hayami, Y. Kamiya, Frustration and chiral orderings in correlated electron systems, Rep. Prog. Phys. 79 (8) (2016) 084504. doi:10.1088/0034-4885/79/8/084504.

[55] S. Hayami, S.-Z. Lin, Y. Kamiya, C. D. Batista, Vortices, skyrmions, and chirality waves in frustrated mott insulators with a quenched periodic array of impurities, Phys. Rev. B 94 (2016) 174420. doi:10.1103/PhysRevB.94.174420.

[56] S.-Z. Lin, C. D. Batista, Face centered cubic and hexagonal close packed skyrmion crystals in centrosymmetric magnets, Phys. Rev. Lett. 120 (2018) 077202. doi:10.1103/PhysRevLett.120.077202.

[57] K. Okigami, R. Yambe, S. Hayami, Engineering a skyrmion crystal in ferromagnetic/antiferromagnetic bilayers based on magnetic frustration mechanism, J. Phys. Soc. Jpn. 91 (10) (2022) 103701. doi:10.7566/JPSJ.91.103701.

[58] P. Nikolić, Dynamics of local magnetic moments induced by itinerant weyl electrons, Phys. Rev. B 103 (2021) 155151. doi:10.1103/PhysRevB.103.155151.

[59] Z. Wang, Y. Su, S.-Z. Lin, C. D. Batista, Skyrmion crystal from rkky interaction mediated by 2d electron gas, Phys. Rev. Lett. 124 (2020) 207201. doi:10.1103/PhysRevLett.124.207201.

[60] K. Mitsumoto, H. Kawamura, Replica symmetry breaking in the rkky skyrmion-crystal system, Phys. Rev. B 104 (2021) 184432. doi:10.1103/PhysRevB.104.184432.

[61] K. Mitsumoto, H. Kawamura, Skyrmion crystal in the rkky system on the two-dimensional triangular lattice, Phys. Rev. B 105 (2022) 094427. doi:10.1103/PhysRevB.105.094427.

[62] R. Ozawa, S. Hayami, Y. Motome, Zero-field skyrmions with a high topological number in itinerant magnets, Phys. Rev. Lett. 118 (2017) 147205. doi:10.1103/PhysRevLett.118.147205.

[63] S. Hayami, R. Ozawa, Y. Motome, Effective bilinear-biquadratic model for noncoplanar ordering in itinerant magnets, Phys. Rev. B 95 (2017) 224424. doi:10.1103/PhysRevB.95.224424.

[64] S. Hayami, Y. Motome, Effect of magnetic anisotropy on skyrmions with a high topological number in itinerant magnets, Phys. Rev. B 99 (2019) 094420. doi:10.1103/PhysRevB.99.094420.

[65] R. Eto, M. Mochizuki, Dynamical switching of magnetic topology in microwave-driven itinerant magnet, Phys. Rev. B 104 (2021) 104425. doi:10.1103/PhysRevB.104.104425.

[66] S. Hayami, Temperature-driven transition from skyrmion to bubble crystals in centrosymmetric itinerant magnets, New J. Phys. 23 (2021) 113032. doi:10.1088/1367-2630/ac3683.

[67] Z. Wang, C. D. Batista, Skyrmion crystals in the triangular kondo lattice model, arXiv:2111.13976 (2021).

[68] R. Eto, R. Pohle, M. Mochizuki, Low-energy excitations of skyrmion crystals in a centrosymmetric kondo-lattice magnet: Decoupled spin-charge excitations and nonreciprocity, Phys. Rev. Lett. 129 (2022) 017201. doi:10.1103/PhysRevLett.129.017201.

[69] D. Amoroso, P. Barone, S. Picozzi, Spontaneous skyrmionic lattice from anisotropic symmetric exchange in a ni-halide monolayer, Nat. Commun. 11 (1) (2020) 5784. doi:10.1038/s41467-020-19535-w.

[70] R. Yambe, S. Hayami, Skyrmion crystals in centrosymmetric itinerant magnets without horizontal mirror plane, Sci. Rep. 11 (2021) 11184. doi:10.1038/s41598-021-90308-1.

[71] S. Hayami, Y. Motome, Square skyrmion crystal in centrosymmetric itinerant magnets, Phys. Rev. B 103 (2021) 024439. doi:10.1103/PhysRevB.103.024439.

[72] S. Hayami, Y. Motome, Noncoplanar multiple-q spin textures by itinerant frustration: Effects of single-ion anisotropy and bond-dependent anisotropy, Phys. Rev. B 103 (2021) 054422. doi:10.1103/PhysRevB.103.054422.

[73] Z. Wang, Y. Su, S.-Z. Lin, C. D. Batista, Meron, skyrmion, and vortex crystals in centrosymmetric tetragonal magnets, Phys. Rev. B 103 (2021) 104408. doi:10.1103/PhysRevB.103.104408.

[74] D. Amoroso, P. Barone, S. Picozzi, Interplay between single-ion and two-ion anisotropies in frustrated 2d semiconductors and tuning of magnetic structures topology, Nanomaterials 11 (8) (2021) 1873. doi:10.3390/nano11081873.

[75] O. I. Utesov, Thermodynamically stable skyrmion lattice in a tetragonal frustrated antiferromagnet with dipolar interaction, Phys. Rev. B 103 (2021) 064414. doi:10.1103/PhysRevB.103.064414.

[76] O. I. Utesov, Mean-field description of skyrmion lattice in hexagonal frustrated antiferromagnets, Phys. Rev. B 105 (2022) 054435. doi:10.1103/PhysRevB.105.054435.

[77] S. Hayami, S.-Z. Lin, C. D. Batista, Bubble and skyrmion crystals in frustrated magnets with easy-axis anisotropy, Phys. Rev. B 93 (2016) 184413. doi:10.1103/PhysRevB.93.184413.

[78] S. Hayami, Rectangular and square skyrmion crystals on a centrosymmetric square lattice with easy-axis anisotropy, Phys. Rev. B 105 (2022) 174437. doi:10.1103/PhysRevB.105.174437.

[79] S. Hayami, Skyrmion crystals in centrosymmetric triangular magnets under hexagonal and trigonal single-ion anisotropy, J. Magn. Magn. Mater. 553 (2022) 169220. doi:10.1016/j.jmmm.2022.169220.

[80] S.-Z. Lin, Skyrmion lattice in centrosymmetric magnets with local dzyaloshinsky-moriya interaction, arXiv:2112.12850 (2021).

[81] S. Hayami, Multifarious skyrmion phases on a trilayer triangular lattice, Phys. Rev. B 105 (2022) 184426. doi:10.1103/PhysRevB.105.184426.

[82] S. Hayami, Skyrmion crystal and spiral phases in centrosymmetric bilayer magnets with staggered dzyaloshinskii-moriya interaction, Phys. Rev. B 105 (2022) 014408. doi:10.1103/PhysRevB.105.014408.

[83] S. Hayami, Square skyrmion crystal in centrosymmetric systems with locally inversion-asymmetric layers, J. Phys.: Condens. Matter 34 (2022) 365802. doi:10.1088/1361-648X/ac7bcb.

[84] S. R. Saha, H. Sugawara, T. D. Matsuda, H. Sato, R. Mallik, E. V. Sampathkumaran, Magnetic anisotropy, first-order-like metamagnetic transitions, and large negative magnetoresistance in single-crystal gd_2pdsi_3, Phys. Rev. B 60 (1999) 12162–12165. doi:10.1103/PhysRevB.60.12162.

[85] T. Kurumaji, T. Nakajima, M. Hirschberger, A. Kikkawa, Y. Yamasaki, H. Sagayama, H. Nakao, Y. Taguchi, T.-h. Arima, Y. Tokura, Skyrmion lattice with a giant topological hall effect in a frustrated triangular-lattice magnet, Science 365 (6456) (2019) 914–918. doi:10.1126/science.aau0968.

[86] E. V. Sampathkumaran, A report of (topological) hall anomaly two decades ago in gd2pdsi3, and its relevance to the history of the field of topological hall effect due to magnetic skyrmions, arXiv:1910.09194 (2019).

[87] M. Hirschberger, T. Nakajima, M. Kriener, T. Kurumaji, L. Spitz, S. Gao, A. Kikkawa, Y. Yamasaki, H. Sagayama, H. Nakao, S. Ohira-Kawamura, Y. Taguchi, T.-h. Arima, Y. Tokura, High-field depinned phase and planar hall effect in the skyrmion host gd_2pdsi_3, Phys. Rev. B 101 (2020) 220401(R). doi:10.1103/PhysRevB.101.220401.

[88] R. Kumar, K. K. Iyer, P. L. Paulose, E. V. Sampathkumaran, Magnetic and transport anomalies in R_2RhSi_3 (r = Gd, tb, and dy) resembling those of the exotic magnetic material Gd_2PdSi_3, Phys. Rev. B 101 (2020) 144440. doi:10.1103/PhysRevB.101.144440.

[89] S. Spachmann, A. Elghandour, M. Frontzek, W. Löser, R. Klingeler, Magnetoelastic coupling and phases in the skyrmion lattice magnet gd_2pdsi_3 discovered by high-resolution dilatometry, Phys. Rev. B 103 (2021) 184424. doi:10.1103/PhysRevB.103.184424.

[90] V. Chandragiri, K. K. Iyer, E. Sampathkumaran, Magnetic behavior of gd3ru4al12, a layered compound with distorted kagomé net, J. Phys.: Condens. Matter 28 (28) (2016) 286002. doi:10.1088/0953-8984/28/28/286002.

[91] S. Nakamura, N. Kabeya, M. Kobayashi, K. Araki, K. Katoh, A. Ochiai, Spin trimer formation in the metallic compound $gd_3ru_4al_{12}$ with a distorted kagome lattice structure, Phys. Rev. B 98 (2018) 054410. doi:10.1103/PhysRevB.98.054410.

[92] M. Hirschberger, T. Nakajima, S. Gao, L. Peng, A. Kikkawa, T. Kurumaji, M. Kriener, Y. Yamasaki, H. Sagayama, H. Nakao, K. Ohishi, K. Kakurai, Y. Taguchi, X. Yu, T.-h. Arima, Y. Tokura, Skyrmion phase and competing magnetic orders on a breathing kagome lattice, Nat. Commun. 10 (1) (2019) 5831. doi:10.1038/s41467-019-13675-4.

[93] M. Hirschberger, S. Hayami, Y. Tokura, Nanometric skyrmion lattice from anisotropic exchange interactions in a centrosymmetric host, New J. Phys. 23 (2021) 023039. doi:10.1088/1367-2630/abdef9.

[94] N. D. Khanh, T. Nakajima, X. Yu, S. Gao, K. Shibata, M. Hirschberger, Y. Yamasaki, H. Sagayama, H. Nakao, L. Peng, K. Nakajima, R. Takagi, T.-h. Arima, Y. Tokura, S. Seki, Nanometric square skyrmion lattice in a centrosymmetric tetragonal magnet, Nat. Nanotechnol. 15 (2020) 444. doi:10.1038/s41565-020-0684-7.

[95] Y. Yasui, C. J. Butler, N. D. Khanh, S. Hayami, T. Nomoto, T. Hanaguri, Y. Motome, R. Arita, T. h. Arima, Y. Tokura, S. Seki, Imaging the coupling between itinerant electrons and localised moments in the centrosymmetric skyrmion magnet $gdru_2si_2$, Nat. Commun. 11 (2020) 5925. doi:10.1038/s41467-020-19751-4.

[96] N. D. Khanh, T. Nakajima, S. Hayami, S. Gao, Y. Yamasaki, H. Sagayama, H. Nakao, R. Takagi, Y. Motome, Y. Tokura, T.-h. Arima, S. Seki, Zoology of multiple-q spin textures in a centrosymmetric tetragonal magnet with itinerant electrons, Adv. Sci. 9 (2022) 2105452. doi:10.1002/advs.202105452.

[97] T. Shang, Y. Xu, D. J. Gawryluk, J. Z. Ma, T. Shiroka, M. Shi, E. Pomjakushina, Anomalous hall resistivity and possible topological hall effect in the $eual_4$ antiferromagnet, Phys. Rev. B 103 (2021) L020405. doi:10.1103/PhysRevB.103.L020405.

[98] K. Kaneko, T. Kawasaki, A. Nakamura, K. Munakata, A. Nakao, T. Hanashima, R. Kiyanagi, T. Ohhara, M. Hedo, T. Nakama, Y. Onuki, Charge-density-wave order and multiple magnetic transitions in divalent europium compound eual4, J. Phys. Soc. Jpn. 90 (6) (2021) 064704. doi:10.7566/JPSJ.90.064704.

[99] R. Takagi, N. Matsuyama, V. Ukleev, L. Yu, J. S. White, S. Francoual, J. R. L. Mardegan, S. Hayami, H. Saito, K. Kaneko, K. Ohishi, Y. Ōnuki, T.-h. Arima, Y. Tokura, T. Nakajima, S. Seki, Square and rhombic lattices of magnetic skyrmions in a centrosymmetric binary compound, Nat. Commun. 13 (2022) 1472. doi:10.1038/s41467-022-29131-9.

[100] X. Y. Zhu, H. Zhang, D. J. Gawryluk, Z. X. Zhen, B. C. Yu, S. L. Ju, W. Xie, D. M. Jiang, W. J. Cheng, Y. Xu, M. Shi, E. Pomjakushina, Q. F. Zhan, T. Shiroka, T. Shang, Spin order and fluctuations in the $eual_4$ and $euga_4$ topological antiferromagnets: A μSR study, Phys. Rev. B 105 (2022) 014423. doi:10.1103/PhysRevB.105.014423.

[101] M. Kakihana, D. Aoki, A. Nakamura, F. Honda, M. Nakashima, Y. Amako, S. Nakamura, T. Sakakibara, M. Hedo, T. Nakama, Y. Onuki, Giant hall resistivity and magnetoresistance in cubic chiral antiferromagnet euptsi, J. Phys. Soc. Jpn. 87 (2) (2018) 023701. doi:10.7566/JPSJ.87.023701.

[102] K. Kaneko, M. D. Frontzek, M. Matsuda, A. Nakao, K. Munakata, T. Ohhara, M. Kakihana, Y. Haga, M. Hedo, T. Nakama, Y. Onuki, Unique helical magnetic order and field-induced phase in trillium lattice antiferromagnet euptsi, J. Phys. Soc. Jpn. 88 (1) (2019) 013702. doi:10.7566/JPSJ.88.013702.

[103] C. Tabata, T. Matsumura, H. Nakao, S. Michimura, M. Kakihana, T. Inami, K. Kaneko, M. Hedo, T. Nakama, Y. Ōnuki, Magnetic field induced triple-q magnetic order in trillium lattice antiferromagnet euptsi studied by resonant x-ray scattering, J. Phys. Soc. Jpn. 88 (9) (2019) 093704. doi:10.7566/JPSJ.88.093704.

[104] M. Kakihana, D. Aoki, A. Nakamura, F. Honda, M. Nakashima, Y. Amako, T. Takeuchi, H. Harima, M. Hedo, T. Nakama, Y. Onuki, Unique magnetic phases in the skyrmion lattice and fermi surface properties in cubic chiral antiferromagnet euptsi, J. Phys. Soc. Jpn. 88 (9) (2019) 094705. doi:10.7566/JPSJ.88.094705.

[105] S. Gao, O. Zaharko, V. Tsurkan, Y. Su, J. S. White, G. S. Tucker, B. Roessli, F. Bourdarot, R. Sibille, D. Chernyshov, T. Fennell, A. Loidl,

C. Rüegg, Spiral spin-liquid and the emergence of a vortex-like state in $MnSc_2S_4$, Nat. Phys. 13 (2) (2017) 157–161. doi:10.1038/nphys3914.

[106] S. Gao, H. D. Rosales, F. A. G. Albarracín, V. Tsurkan, G. Kaur, T. Fennell, P. Steffens, M. Boehm, P. Čermák, A. Schneidewind, E. Ressouche, D. C. Cabra, C. Rüegg, Z. Oksana, Fractional antiferromagnetic skyrmion lattice induced by anisotropic couplings, Nature 586 (2020) 37–41. doi:10.1038/s41586-020-2716-8.

[107] K. Guratinder, V. Tsurkan, L. Prodan, L. Keller, J. P. Embs, F. Juranyi, M. Medarde, C. Rüegg, O. Zaharko, Magnetic order and exchange coupling in the frustrated diamond-lattice antiferromagnet $mnsc_2se_4$, Phys. Rev. B 105 (2022) 174423. doi:10.1103/PhysRevB.105.174423.

[108] H. D. Rosales, F. A. G. Albarracín, K. Guratinder, V. Tsurkan, L. Prodan, E. Ressouche, O. Zaharko, Anisotropy-driven response of the fractional antiferromagnetic skyrmion lattice in $mnsc_2s_4$ to applied magnetic fields, Phys. Rev. B 105 (2022) 224402. doi:10.1103/PhysRevB.105.224402.

[109] S. Mühlbauer, B. Binz, F. Jonietz, C. Pfleiderer, A. Rosch, A. Neubauer, R. Georgii, P. Böni, Skyrmion lattice in a chiral magnet, Science 323 (5916) (2009) 915–919. doi:10.1126/science.1166767.

[110] K. Karube, J. S. White, D. Morikawa, M. Bartkowiak, A. Kikkawa, Y. Tokunaga, T. Arima, H. M. Rønnow, Y. Tokura, Y. Taguchi, Skyrmion formation in a bulk chiral magnet at zero magnetic field and above room temperature, Phys. Rev. Materials 1 (2017) 074405. doi:10.1103/PhysRevMaterials.1.074405.

[111] J. C. Gallagher, K. Y. Meng, J. T. Brangham, H. L. Wang, B. D. Esser, D. W. McComb, F. Y. Yang, Robust zero-field skyrmion formation in fege epitaxial thin films, Phys. Rev. Lett. 118 (2017) 027201. doi:10.1103/PhysRevLett.118.027201.

[112] M. He, L. Peng, Z. Zhu, G. Li, J. Cai, J. Li, H. Wei, L. Gu, S. Wang, T. Zhao, et al., Realization of zero-field skyrmions with high-density via electromagnetic manipulation in pt/co/ta multilayers, Appl. Phys. Lett. 111 (20) (2017) 202403. doi:doi.org/10.1063/1.5001322.

[113] L. Peng, Y. Zhang, W. Wang, M. He, L. Li, B. Ding, J. Li, Y. Sun, X.-G. Zhang, J. Cai, et al., Real-space observation of nonvolatile zero-field biskyrmion lattice generation in mnniga magnet, Nano Lett. 17 (11) (2017) 7075–7079. doi:10.1021/acs.nanolett.7b03792.

[114] Y. Guang, I. Bykova, Y. Liu, G. Yu, E. Goering, M. Weigand, J. Gräfe, S. K. Kim, J. Zhang, H. Zhang, Z. Yan, C. Wan, J. Feng, X. Wang, C. Guo, H. Wei, Y. Peng, Y. Tserkovnyak, X. Han, G. Schütz, Creating zero-field skyrmions in exchange-biased multilayers through x-ray illumination, Nat. Commun. 11 (1) (2020) 949. doi:10.1038/s41467-020-14769-0.

[115] M. Li, A. Rai, A. Pokhrel, A. Sapkota, C. Mewes, T. Mewes, M. D. Graef, V. Sokalski, Formation of zero-field skyrmion arrays in asymmetric superlattices, Appl. Phys. Lett. 117 (11) (2020) 112403. doi:10.1063/5.0024265.

[116] S. Hayami, R. Yambe, Meron-antimeron crystals in noncentrosymmetric itinerant magnets on a triangular lattice, Phys. Rev. B 104 (2021) 094425. doi:10.1103/PhysRevB.104.094425.

[117] S. Hayami, Multiple skyrmion crystal phases by itinerant frustration in centrosymmetric tetragonal magnets, J. Phys. Soc. Jpn. 91 (2) (2022) 023705. doi:10.7566/JPSJ.91.023705.

[118] The Hamiltonian in momentum space in Eq. (1) is related to that in real space as $\mathcal{H} = \sum_{ij} J_{ij} I_{ij}^{\alpha\beta} S_i^\alpha S_j^\beta$, where J_{ij} stands for the interaction between ith spin and jth spin.

[119] M. Becker, M. Hermanns, B. Bauer, M. Garst, S. Trebst, Spin-orbit physics of $j = \frac{1}{2}$ mott insulators on the triangular lattice, Phys. Rev. B 91 (2015) 155135. doi:10.1103/PhysRevB.91.155135.

[120] M. Li, N. B. Perkins, I. Rousochatzakis, Collective spin dynamics of F_2 vortex crystals in triangular kitaev-heisenberg antiferromagnets, Phys. Rev. Research 1 (2019) 013002. doi:10.1103/PhysRevResearch.1.013002.

[121] S. Hayami, Y. Motome, Néel- and bloch-type magnetic vortices in rashba metals, Phys. Rev. Lett. 121 (2018) 137202. doi:10.1103/PhysRevLett.121.137202.

[122] S. Hayami, Y. Motome, Multiple-q magnetic states in spin-orbit coupled metals, IEEE Transactions on Magnetics 55 (99) (2019) 1500107. doi:10.1109/TMAG.2018.2860999.

[123] S. Hayami, R. Yambe, Degeneracy lifting of néel, bloch, and anti-skyrmion crystals in centrosymmetric tetragonal systems, J. Phys. Soc. Jpn. 89 (10) (2020) 103702. doi:10.7566/JPSJ.89.103702.

[124] Y. Kato, S. Hayami, Y. Motome, Spin excitation spectra in helimagnetic states: Proper-screw, cycloid, vortex-crystal, and hedgehog lattices, Phys. Rev. B 104 (2021) 224405. doi:10.1103/PhysRevB.104.224405.

[125] S. Hayami, R. Yambe, Helicity locking of a square skyrmion crystal in a centrosymmetric lattice system without vertical mirror symmetry, Phys. Rev. B 105 (2022) 104428. doi:10.1103/PhysRevB.105.104428.

[126] S. Hayami, Stability of skyrmion crystal phase in centrosymmetric distorted triangular-lattice antiferromagnets, J. Phys. Soc. Jpn. 91 (9) (2022) 093701. doi:10.7566/JPSJ.91.093701.

[127] M. A. Ruderman, C. Kittel, Indirect exchange coupling of nuclear magnetic moments by conduction electrons, Phys. Rev. 96 (1954) 99–102. doi:10.1103/PhysRev.96.99.

[128] T. Kasuya, A theory of metallic ferro- and antiferromagnetism on zener's model, Prog. Theor. Phys. 16 (1) (1956) 45–57. doi:10.1143/PTP.16.45.

[129] K. Yosida, Magnetic properties of cu-mn alloys, Phys. Rev. 106 (1957) 893–898. doi:10.1103/PhysRev.106.893.

[130] S. Hayami, In-plane magnetic field-induced skyrmion crystal in frustrated magnets with easy-plane anisotropy, Phys. Rev. B 103 (2021) 224418. doi:10.1103/PhysRevB.103.224418.

[131] S. Hayami, Skyrmion crystal with integer and fractional skyrmion numbers in a nonsymmorphic lattice structure with the screw axis, Phys. Rev. B 105 (2022) 224411. doi:10.1103/PhysRevB.105.224411.

[132] S. Hayami, Multiple-q magnetism by anisotropic bilinear-biquadratic interactions in momentum space, J. Magn. Magn. Mater. 513 (2020) 167181. doi:10.1016/j.jmmm.2020.167181.

[133] S. Hayami, R. Yambe, Field-direction sensitive skyrmion crystals in cubic chiral systems: Implication to 4f-electron compound euptsi, J. Phys. Soc. Jpn. 90 (7) (2021) 073705. doi:10.7566/JPSJ.90.073705.

[134] R. Yambe, S. Hayami, Effective spin model in momentum space: Toward a systematic understanding of multiple-q instability by momentum-resolved anisotropic exchange interactions, arXiv:2202.09744 (2022).

[135] Y. Kato, Y. Motome, Magnetic field–temperature phase diagrams for multiple-q magnetic ordering: Exact steepest descent approach to long-range interacting spin systems, Phys. Rev. B 105 (2022) 174413. doi:10.1103/PhysRevB.105.174413.

[136] N. Metropolis, A. W. Rosenbluth, M. N. Rosenbluth, A. H. Teller, E. Teller, Equation of state calculations by fast computing machines, J. Chem. Phys. 21 (6) (1953) 1087–1092.

[137] D. Solenov, D. Mozyrsky, I. Martin, Chirality waves in two-dimensional magnets, Phys. Rev. Lett. 108 (2012) 096403. doi:10.1103/PhysRevLett.108.096403.

[138] R. Ozawa, S. Hayami, K. Barros, G.-W. Chern, Y. Motome, C. D. Batista, Vortex crystals with chiral stripes in itinerant magnets, J. Phys. Soc. Jpn. 85 (10) (2016) 103703. doi:10.7566/JPSJ.85.103703.

[139] S. Okumura, S. Hayami, Y. Kato, Y. Motome, Magnetic hedgehog lattice in a centrosymmetric cubic metal, J. Phys. Soc. Jpn. 91 (9) (2022) 093702. doi:10.7566/JPSJ.91.093702.

[140] R. Yambe, S. Hayami, Double-q chiral stripe in the d–p model with strong spin–charge coupling, J. Phys. Soc. Jpn. 89 (1) (2020) 013702. doi:10.7566/JPSJ.89.013702.

[141] L. Brey, H. Fertig, R. Côté, A. MacDonald, Skyrme and meron crystals in quantum hall ferromagnets, Phys. Scr. 1996 (T66) (1996) 154. doi:10.1088/0031-8949/1996/T66/027.

[142] M. Ezawa, Compact merons and skyrmions in thin chiral magnetic films, Phys. Rev. B 83 (2011) 100408(R). doi:10.1103/PhysRevB.83.100408.

[143] S.-Z. Lin, A. Saxena, C. D. Batista, Skyrmion fractionalization and merons in chiral magnets with easy-plane anisotropy, Phys. Rev. B 91 (2015) 224407. doi:10.1103/PhysRevB.91.224407.

[144] A. Tan, J. Li, A. Scholl, E. Arenholz, A. T. Young, Q. Li, C. Hwang, Z. Q. Qiu, Topology of spin meron pairs in coupled ni/fe/co/cu(001) disks, Phys. Rev. B 94 (2016) 014433. doi:10.1103/PhysRevB.94.014433.

[145] S. Bera, S. S. Mandal, Theory of the skyrmion, meron, antiskyrmion, and antimeron in chiral magnets, Phys. Rev. Research 1 (2019) 033109. doi:10.1103/PhysRevResearch.1.033109.

[146] S. Hayami, R. Yambe, Locking of skyrmion cores on a centrosymmetric discrete lattice: Onsite versus offsite, Phys. Rev. Research 3 (2021) 043158. doi:10.1103/PhysRevResearch.3.043158.

[147] Y. Kamiya, C. D. Batista, Magnetic vortex crystals in frustrated mott insulator, Phys. Rev. X 4 (2014) 011023. doi:10.1103/PhysRevX.4.011023.